NeuroImage 81 (2013) 96–109

Contents lists available at SciVerse ScienceDirect

NeuroImage

journal homepage: www.elsevier.com/locate/ynimg

Selectively and progressively disrupted structural connectivity of functional brain networks in Alzheimer's disease — Revealed by a novel framework to analyze edge distributions of networks detecting disruptions with strong statistical evidence

Klaus Hahn [a,*], Nicholas Myers [b,c], Sergei Prigarin [e], Karsten Rodenacker [a], Alexander Kurz [b], Hans Förstl [b], Claus Zimmer [c], Afra M. Wohlschläger [c,d], Christian Sorg [b,c]

[a] Institute of Computational Biology, Helmholtz Zentrum München, German Research Center for Environmental Health, Ingolstaedter Landstrasse 1, 85764 Neuherberg, Germany
[b] Department of Psychiatry, Technische Universität München, Ismaningerstrasse 22, 81675 Munich, Germany
[c] Department of Neuroradiology, Technische Universität München, Ismaningerstrasse 22, 81675 Munich, Germany
[d] Department of Neurology of Klinikum rechts der Isar, Technische Universität München, Ismaningerstrasse 22, 81675 Munich, Germany
[e] Institute of Computational Mathematics and Mathematical Geophysics, Siberian Branch of Russian Academy of Sciences, pr. Lavrentieva 6, Novosibirsk 630090, Russia

ARTICLE INFO

Article history:
Accepted 1 May 2013
Available online 11 May 2013

Keywords:
Multimodal fMRI/DTI analysis of Alzheimer's disease
Intrinsic functional brain networks
Structural connectivity networks
Edge frequency distributions
Nonparametric Brunner statistic

ABSTRACT

Alzheimer's disease (AD) disrupts selectively and progressively (increasing with severity) functional connectivity of intrinsic brain networks (IBNs), most prominent in the default mode network. Given that IBNs' functional connectivity depends on structural connectivity, we hypothesize for our study selective and progressive changes of IBN based structural connectivity in AD. To achieve strong statistical evidence, we introduce a novel statistical method based on the edge frequency distributions of structural connectivity networks. Such non-Gaussian distributions are compared in a multiple testing scheme, combining a flexible nonparametric test statistic with permutation based strong control of the family wise error rate. We assessed 26 healthy elderly, 23 patients with AD-dementia, and 28 patients with mild cognitive impairment (MCI) by resting-state functional MRI, diffusion tensor imaging, and clinical–neuropsychological testing including annual follow-up assessment. After 3 years, 50% of the patients with MCI converted to AD. Tractography of diffusion tensor data identifies structural connectivity networks between regions of IBNs, which are detected by an independent component analysis of resting state fMRI data. We find that IBNs' structural connectivity is selectively and progressively disrupted with primary changes in the default mode network. Correspondent results are found for IBNs' functional connectivity. In addition, structural connectivity across the nodes of all IBNs separated individual MCI patients converting to AD from non-converters. Conclusively, our study provides a new approach to analyze connectivity networks by their non-Gaussian edge frequency distributions and achieves strong statistical evidence by application of the family wise error rate. Data analysis provides selective and progressive disruptions of IBN's structural connectivity in AD and demonstrates the increased power of our method compared to recent studies.

Introduction

Alzheimer's disease (AD) is the most frequent neurodegenerative disease that causes more than 60% of age-related dementia (Blennow et al., 2006). Brain changes associated with AD are widespread, they concern different spatial levels and modalities, and they proceed in specific temporospatial pattern (e.g. Bateman et al., 2012; Ewers et al., 2011). For example amyloid plaques, which are essential for AD pathology (Blennow et al., 2006), start very early in asymptomatic stages of the disease at neocortical sites and spread out across the whole brain, while neurofibrillary tangles and cell loss start later, mostly in the entorhinal cortex and hippocampus accompanied by first cognitive symptoms (Braak and Braak, 1991). To understand AD's pathogenesis, it is important to understand how these different types of changes propagate and relate among each other. The current study contributes to that kind of question by focusing on large-scale brain connectivity.

A very consistent finding in AD is the selective and progressive (increasing with severity) disruption of functional connectivity of intrinsic brain networks (IBNs) (Agosta et al., 2012; Greicius et al., 2004; Sorg et al., 2007, 2009). IBNs are characterized by synchronous ongoing brain activity and constitute a basic form of large-scale brain organization (Fox and Raichle, 2007; Smith et al., 2009). In AD functional connectivity changes of IBN start before the first cognitive

* Corresponding author at: Institute of Computational Biology, Helmholtz Zentrum München, German Research Center for Environmental Health, Ingolstaedter Landstrasse 1, 85764 Neuherberg, Germany. Fax: +49 8931873369.
E-mail address: hahn@helmholtz-muenchen.de (K. Hahn).

1053-8119/$ – see front matter © 2013 Elsevier Inc. All rights reserved.
http://dx.doi.org/10.1016/j.neuroimage.2013.05.011

symptoms are present, they primarily concern the default mode network (DN) and they are associated with the spatial distribution of amyloid plaques, indicating their association with AD's critical pathology (Drzezga et al., 2011; Mormino et al., 2011; Sperling et al., 2009). Since functional connectivity of ongoing brain activity depends on fiber-based structural connectivity (Greicius et al., 2009; Hagmann et al., 2008; van den Heuvel et al., 2009), the question arises whether functional connectivity disruptions of IBNs reflect at least partly structural connectivity disruptions of IBNs in AD. Previous diffusion tensor imaging (DTI) studies in patients with AD dementia or mild cognitive impairment MCI (MCI, a risk-state for AD (Gauthier et al., 2006)) demonstrate widely distributed and progressive changes of white matter fibers (e.g. Bozzali et al., 2011; Fellgiebel et al., 2005; Lo et al., 2010; Stahl et al., 2007; for review Sexton et al., 2011); these changes have a biomarker potential (Deppe et al., 2007; Duning et al., 2009; Shao et al., 2012), and, importantly, they overlap with structural connections of several IBNs (Hagmann et al., 2008). These findings suggest that disrupted structural connectivity is associated with disrupted functional connectivity of IBNs in AD. However, explicit evidence for disrupted structural connectivity of IBNs in AD beyond simple spatial overlap is still missing. In particular, it is unknown how structural connectivity disruptions are distributed (selectivity) across IBNs and proceed (progression) in the transition from healthy control to MCI and AD, and whether they correspond with changes of functional connectivity in IBNs.

To be able to get such evidence, we performed a multimodal imaging approach (including resting-state functional MRI (rs-fMRI) and DTI) to detect IBNs and their structural connectivity networks. To get strong statistical evidence for the results of our data analysis, a novel method – which might be of general interest for the analysis of brain networks – is applied: To identify changes of structural connectivity within a given IBN the connectivity strengths (or weighted edges) of the corresponding structural network are collected in a univariate sample. Such samples define frequency distributions, which are subsequently used for comparison across subjects (group–group and subject–group comparisons are performed). To account for these highly skewed and multimodal univariate distributions, novel procedures of nonparametric statistics are necessary; we used a statistic proposed by Brunner and Munzel (2000, 2002). To achieve strong evidence for this statistic, adjusted P-values controlling the "family wise error rate in the strong sense" were calculated according to a recent method by Westfall and Troendle (2008).

The following hypotheses were addressed in our statistical tests: (i) AD disrupts selectively and progressively structural connectivity of IBNs, primarily that of the DN. (ii) For IBNs, disrupted structural connectivity corresponds with disrupted functional connectivity. (iii) Structural connectivity reductions of IBNs indicate AD at single subject level in already pre-dementia stages of the disease.

Only few studies on connectivity in Alzheimer use the multimodal coupling of rs-fMRI and DTI (Soldner et al., 2012; Wee et al., 2012; Zhou et al., 2008). Soldner et al. apply a "Region-of-interest (ROI) analysis" to study modifications in connectivity in Alzheimer. ROIs in white matter and in the neighboring cortex are defined manually to indicate changes of structural and functional connectivity; after Bonferroni correction significant changes of structural connectivity between healthy control and AD could be detected in posterior cingulate fibers of the left hemisphere, functional connectivity was not significantly changed. Wee et al. merge whole brain functional (rs-fMRI) and structural (DTI) connectivity networks by "Support Vector Machines" to achieve improved classification performance for MCI or early-AD identification; they show that multimodality improves the classification accuracy compared to the use of the single modalities. Zhou et al. focused on the DN's connectivity. In a smaller group of patients they found (on the basis of unadjusted P-values) reduced structural connectivity of the hippocampus and posterior cingulate cortex into the whole brain, both areas are DN hubs and are also covered in our essentially enlarged study. P-values for changes of functional connectivity in patients with AD dementia are not given.

Materials and methods

Subjects

23 patients with mild AD dementia (69.7 years ± 8.1, 10 females), 28 patients with MCI (69.5 ± 7.1, 14 females) and 26 healthy controls (HC; 65.5 ± 7.8, 16 females) participate in this study (Table 1). All participants provided informed consent in accordance with the Human Research Committee guidelines of the Klinikum Rechts der Isar, Technische Universität, München. Patients were recruited from the Memory Clinic of the Department of Psychiatry, healthy controls by word-of-mouth advertising. Examination of every participant included medical history, neurological examination, neuropsychological assessment (Consortium to establish a registry for AD, CERAD (Morris et al., 1989)), structural MRI, and informant interview (Clinical Dementia Rating, CDR (Morris, 1993)) as well as only for patient blood tests. Patients with mild AD fulfill criteria for dementia (CDR global score = 1) and the NINCDS–ADRDA criteria for AD (McKhann et al., 1984). Patients with MCI met criteria for MCI including reported and neuropsychologically assessed cognitive impairments, largely intact activities of daily living, and excluded dementia (CDR = 0.5) (Gauthier et al., 2006). For these MCI patients, potential conversion to AD dementia was evaluated by annual follow-up clinical assessments over 3 years after baseline including medical history, neurological examination, informant interview (CDR), and neuropsychological assessment (CERAD) (MCI-c — MCI-converter, MCI-nc — MCI-non-converter). Three patients converted to AD after one year (cases 21, 27, 35 of Fig. 5/B), 5 after 2 (cases 4, 7, 12, 17, 30 of Fig. 5/B), and 5 after 3 (cases 2, 6, 9, 11, 34 of Fig. 5/B). Exclusion criteria for entry into the study were other neurological, psychiatric, or systemic diseases (e.g., stroke, depression, alcoholism) or clinically remarkable MRI (e.g., stroke lesions) potentially related to cognitive impairment. 9/7/5/11 patients with mild AD/MCI-c/MCI-nc/controls were treated

Table 1
Demographical and neuropsychological data of patients and healthy controls.

Group	HC (n = 26)	AD (n = 23)	MCI (n = 28)	MCI-c (n = 13)	MCI-nc (n = 15)	P
Gender						
Female	16	10	14	6	8	0.21
Male	10	13	14	7	7	
Age	65.5 ± 7.8	69.7 ± 8.1	69.5 ± 7.1	72.0 ± 7.0	67.4 ± 6.9	0.42
Years of education	12.4 ± 2.3	11.9 ± 3.2	12.0 ± 3.0	11.8 ± 2.9	12.1 ± 3.0	0.23
CDR-SB	0.2 ± 0.53	5.7 ± 1.9	2.9 ± 1.3	3.0 ± 1.4	2.9 ± 1.4	<0.01
MMSE score	29.5 ± 0.8	22.3 ± 3.9	26.7 ± 1.9	26.3 ± 2.3	27.0 ± 1.8	<0.01
Delayed recall (CERAD)	8.5 ± 2.2	1.3 ± 1.8	3.0 ± 1.3	2.4 ± 1.5	3.6 ± 1.5	<0.01

HC: healthy controls; AD: Alzheimer's disease; MCI: mild cognitive impairment; CDR-SB: Clinical Dementia Rating Sum-of-the-Boxes; MMSE: Mini-Mental-State-Examination; CERAD: Consortium to Establish Registry for AD; P: P-values concerning only group comparisons across HC, mild AD, and MCI; for statistical evaluation of group comparison: χ^2 (gender) and ANOVA (age, education, CDR-SB, MMSE, delayed recall).

for hypertension (beta-blockers, ACE-inhibitors, calcium channel blockers), 5/4/6/10 for hypercholesterolemia (statins). 3/2/0/0 individuals had diabetes mellitus, 4/3/2/0 receive antidepressant medication (mirtazapine, escitalopram, fluoxetine), and all patients with mild AD received cholinesterase inhibitors. Controls were free of any psychotropic medication.

Data acquisition

Using 3 T-MRI scanner (Achieva, Philips), we acquired diffusion weighted images (DWIs) for pulsed gradient spin-echo echo planar imaging sequence with a parallel imaging (SENSE) factor of 2.5, TE = 60 ms, and TR = 6516 ms. Images were acquired for 112 × 112 matrix size per slice and subsequently reconstructed for a 128 × 128 matrix size, with a resolution of 1.75 mm in plane and a slice thickness of 2 mm. A total of 60 contiguous slices was acquired to give complete brain coverage containing 128 × 128 × 60 voxels with size 1.75 × 1.75 × 2 mm^3. Diffusion gradients were applied in 15 non-collinear directions with b = 800 s/mm^2. B0 image without diffusion weighting, b = 0 s/mm^2, was additionally acquired. For co-registration, T1-weighted anatomical data were obtained by using a magnetization-prepared rapid acquisition gradient echo sequence (TE = 4 ms, TR = 9 ms, TI = 100 ms, flip angle = 5°, FoV =240 × 240 mm^2, matrix = 240 × 240, 170 slices, voxel size =1 × 1 × 1 mm^3). Rs-fMRI data were collected using a gradient echo EPI sequence (TE = 35 ms, TR = 2000 ms, flip angle = 82°, FoV = 220 × 220 mm^2, matrix = 80 × 80, 32 slices, slice thickness = 4 mm, and 0 mm interslice gap; 10 min of scanning resulted in 300 images).

Resting state-fMRI data analysis: IBNs and definition of gray matter ROIs for structural connectivity

Preprocessing and independent component analysis

To define IBNs, we applied canonical independent component analysis (ICA) to rs-fMRI data. For each participant the first three volumes of rs-fMRI-session were discarded due to magnetization effects. SPM8 (Wellcome Department of Cognitive Neurology, London) was used for motion correction, spatial normalization into the stereotactic space of the Montreal Neurological Institute (MNI) and spatial smoothing with an 8 × 8 × 8 mm Gaussian kernel. Subsequently, data were decomposed by an ICA approach (e.g. Sorg et al., 2007). More specifically, preprocessed data of all subjects were decomposed into 41 spatial independent components within a group-ICA framework (Calhoun et al., 2001), which is based on the infomax-algorithm and implemented in the GIFT-software (http://icatb.sourceforge.net). Dimensionality estimation was performed by using the minimum description length criteria and resulted in the 41 components representing the mean of all individual estimates. Before volumes were entered into ICA analysis, voxel-wise z-transformation on time course data $y_{ijk}(t)$ was applied by subtracting the mean $<y_{ijk}>$ and dividing by the standard deviation σ_{ijk} ($\hat{y}_{ijk}(t) = (y_{ijk}(t) - <y_{ijk}>) / \sigma_{ijk}$), (t time, *i,j,k* directions in space). The sensitivity of the multivariate ICA algorithm for correlation of variance between voxels, i.e. functional connectivity, was thereby rendered independent of the original BOLD signal magnitude across subjects. Data were concatenated and reduced by two-step principal component analysis (PCA), followed by independent component estimation with the infomax-algorithm. This resulted in a set of average group components, which were then back reconstructed into single subject space. Each back-reconstructed component consisted of a spatial z-map reflecting component's functional connectivity pattern across space and an associated time course reflecting component's activity across time. Before we entered the individual's spatial maps into second-level statistics we reintegrated the initially calculated scaling factor σ_{ijk} into the data by voxel-wise multiplication in order to preserve each individual's profile of variance magnitude while leaving the normalized time course component unchanged. Only spatial z-maps were used for further analysis.

IBNs of interest

Independent components reflecting IBNs of interest were identified by visual inspection of two independent raters (A.W., C.S.). IBNs of interest were the anterior and posterior DN (aDN, pDN), dorsal and ventral attention networks (dAN, vAN), and the left and right lateralized executive control networks (lEN, rEN), which all include brain regions consistently affected by AD (e.g. Buckner et al., 2009; Drzezga et al., 2011; Sorg et al., 2009). To control for AD's selective effects, primary sensorimotor (SMN) and visual networks (VN), which are usually not affected by early AD, were also included.

Statistical evaluation

To evaluate the spatial consistency of IBNs, we calculated voxel-wise one-sample t-tests on participants' reconstructed spatial maps across all subjects for each IBN. The resulting statistical parametric maps (SPM) were thresholded and corrected for multiple testing ($P < 0.05$, FDR (false discovery rate) corrected). We then examined group differences for spatial maps of intrinsic functional connectivity for each IBN. Individual maps were entered into voxel-wise analysis of variance (ANOVA) and a conjunction map of the one-sample t-test image ($P < 0.001$ uncorrected) was applied as a mask to the analysis. Post-hoc two-sample t-tests were used to evaluate direction of changes. All resulting SPMs were thresholded and corrected for multiple testing ($P < 0.05$, FDR).

Defining IBN-ROIs for structural analysis

Peak coordinates of significant clusters of one-sample t-tests were used to define critical voxels in IBNs. These voxels were used as ROI-centers (spherical shape with radius = 9 mm) for the structural connectivity analysis. Due to its relevance for AD (Sorg et al., 2009), we further included the left and right anterior and posterior hippocampus defined by the Anatomy Toolbox (Wellcome Department of Cognitive Neurology, London) in SPM and converted them to correspondent ROIs using MarsBaR (http://marsbar.sourceforge.net).

Voxel-based morphometry (VBM) analysis

To evaluate potential effects of atrophy on IBN functional connectivity changes, additional VBM of T1-weighted MRI data was performed. As described recently (Sorg et al., 2013), we used the VBM8 toolbox (http://dbm.neuro.uni-jena.de/vbm.html) to analyze brain structure. T1-weighted images were corrected for bias-field inhomogeneity, registered using linear (12-parameter affine) and nonlinear transformations, and tissue-classified into gray matter (GM), white matter, and cerebro-spinal fluid within the same generative model. The resulting GM images were modulated to account for volume changes resulting from the normalization process. Here, we only considered non-linear volume changes so that further analyses did not have to account for differences in head size. Finally images were smoothed with a Gaussian kernel of 8 mm (FWHM). For group comparisons, voxel-wise ANOVA was performed ($P < 0.05$ FWE corrected).

DTI data analysis: post-processing and construction of structural connectivity matrices

Post-processing

Noise in DWIs was reduced by edge preserving spatial filtering. A chain of nonlinear Gaussian filters was applied to every weighted and b = 0 image (Hahn et al., 2010). Distortions in DWIs due to eddy-currents and head movement were corrected by affine registration to the b = 0 image using FSL-software (www.fmrib.ox.ac.uk/fsl). The standard diffusion tensor model with six independent components was then fitted to the corrected DWIs for each voxel by the following procedure: First, logarithmic linear least squares estimation (LLS)

based on the Stejskal–Tanner equations (Basser and Jones, 2002) was applied. These estimated tensors were then used as seed points in a second estimation to improve positive definiteness of the tensors. For this purpose, a penalized nonlinear least squares estimation (PNLS) was performed, where the Sylvester condition for the tensor D was used in the penalty term. Formally PNLS is given by

$$\min_D \left\{ \frac{1}{15}\sum_{i=1}^{15}\left(S_i/S_0 - e^{-b\langle g_i|D|g_i\rangle}\right)^2 + k*\left\{\min(d_1,0)^2 + \min(\det[D_1],0)^2 + \min(\det[D],0)^2\right\}\right\}$$

for $k >> 1, D_1 = \begin{bmatrix} d_1 & d_4 \\ d_4 & d_2 \end{bmatrix}, D = \begin{bmatrix} d_1 & d_4 & d_5 \\ d_4 & d_2 & d_6 \\ d_5 & d_6 & d_3 \end{bmatrix}, S_i$ are the DWIs,

S_0 the b = 0 image, $|g_i\rangle$the gradients and b diffusion weighting.

PNLS is conceptually equivalent to the constrained nonlinear least squares estimation (CNLS) proposed by Koay et al. (2006), but differs numerically, as for non-positive definite seed tensors an approximate (modified) Cholesky decomposition is not necessary; the price to pay is that for PNLS a global minimizer must be used. This numerical technique was introduced, in detail described and validated for the two-tensor model in Hahn et al. (2013), but it is equally applicable to standard model estimations. For validation, Monte Carlo simulations with the same model parameters as applied for Figs. 5/6 in Koay et al. (2006) were performed; our results are given in Table 2 and show clearly an improvement for the mean squared errors of FA and for the TRACE values. In addition, the fraction of converters to positive tensors (achieved by PNLS) against tensors with negative eigenvalues (achieved by LLS alone) is given.

For each subject the IBN-ROIs were mapped from MNI space to individual's b = 0 image of DWI-space by affine transformations. Transformations were based on registration of individual T1 images to the ICBM152 T1 template (http://www.bic.mni.mcgill.ca) and the co-registration of individual T1 images and b = 0 images. The ROIs were then reduced to volumes without cerebral spinal fluid and with FA ≤ 0.1 indicating gray matter. Finally, voxel size of DTI space was reduced to isotropic 1 mm^3 voxels applying Log-Euclidian interpolation (Arsigny et al., 2006) or, in regions where positive definiteness of the tensors could not be achieved, by trilinear interpolation (Hill and Batchelor, 2001).

Tractography and connectivity strength

To calculate the structural connectivity between any pair of gray matter ROIs for each subject, we applied the deterministic tracking method TEND (Lazar et al., 2003) with a fixed step length of 0.5 mm. TEND uses the whole tensor for the propagation of tracks and is less sensitive to artifacts than e.g. the Streamline method. From every interpolated white matter voxel with FA > 0.1 randomly 100 seed points were chosen following the brute force method. From these seed points for both orientations of the principal diffusion a fiber track was calculated, summing up for the whole brain to ~10^8 fibers. The propagation of a fiber was stopped for one of three conditions: 1) The angle between consecutive path segments is above 30°; 2) the fiber enters gray matter (FA < 0.1); and 3) the fiber enters CSF (MD > 0.002 mm^2/s). Fibers were discarded completely if their length was beyond a cut-off Δ =25 cm (approximating the maximum length of cortico-cortical fibers). In Fig. 2 examples for TEND tractography are presented. Panel A) gives an axial view of corpus callosum fibers (from a control subject) for few selected seed points chosen along the red line, panel B) presents the corresponding sagittal view. Panel C) shows the sagittal view of fibers calculated with brute force seeding restricted to a 3D volume; the volume is schematically indicated in panel B) by the red rectangle and has an axial thickness of 4 mm; in every WM voxel (size 1 mm^3) within this seed volume two fibers were started at random positions; please note the high density of fibers indicating connectivity between the two cerebral hemispheres (to keep the figure transparent, fibers below the seed volume were discarded). The fibers of panel C) are only a subset of the corpus callosum fibers involved in our study, as the actual corpus callosum seed volume covers the whole corpus callosum and within every such WM voxel 100 tracks are started.

A relative connectivity strength c_{AB} between two ROIs A and B was defined by

$$c_{AB} = \frac{2}{\sum_{j=1}^{n_A} 1/l_j + \sum_{k=1}^{n_B} 1/l_k} \sum_{i=1}^{n_{AB}} 1/l_i, c_{AB} \in [0,1],$$

where n_{AB}, n_A and n_B are the numbers of all calculated fibers connecting A and B, or entering A or B; l_m is the length of fiber m. The measure c_{AB} reflects the connection probability for ROIs A and B (i.e. the probability that fibers connect the ROIs A and B). It includes a correction of a bias caused by the length of fibers (first introduced by Hagmann et al. (2008) to prevent multiple counting of fibers). The quantities $\sum_{i=1}^{n_{AB}} 1/l_i$, $\sum_{j=1}^{n_A} 1/l_j$ and $\sum_{k=1}^{n_B} 1/l_k$ are proportional to the number of connecting or entering fibers after bias correction. This bias is a consequence of brute force seeding and must be corrected for the following reason: Increasing e.g. the length of the fibers between two ROIs A and B (stretching the axons), increases the number of seed points along these fibers and consequently the number of connecting fibers, though connectivity should remain unchanged.

Since there is no general agreement about a "best" measure of connectivity strength, we controlled the dependence of our results on the applied connectivity measure by using a different measure called connection density (Hagmann et al., 2008). Connection density is defined by

$$c_{AB} = \frac{2}{F\_A + F\_B} \sum_{i=1}^{n_{AB}} 1/l_i,$$

where F_A and F_B are the sizes of that part of the ROI-surfaces which separate gray and white matter.

Connectivity matrices: TSBN and SIBN

In Fig. 3/A a spatial scheme of all pairwise connections in the brain between the gray matter ROIs of the 8 IBNs and of the hippocampus is

Table 2
Testing the tensor fitting method PNLS by Monte Carlo simulations.

	MSE FA	MSE TRACE	RATIO CONV/NEG	
$SNR_0 = 5$	$1.35 * 10^{-4}$	$7 * 10^{-9}$		LLS
$FA_{model} = 0.962$	$1.7 * 10^{-5}$	$7 * 10^{-8}$	3358/3415	PNLS
$SNR_0 = 10$	$2 * 10^{-5}$	$2 * 10^{-9}$		LLS
$FA_{model} = 0.962$	$9 * 10^{-6}$	$3 * 10^{-8}$	1559/1562	PNLS
$SNR_0 = 20$	$3.9 * 10^{-6}$	$5 * 10^{-10}$		LLS
$FA_{model} = 0.962$	$3.5 * 10^{-6}$	$5 * 10^{-9}$	205/205	PNLS
$SNR_0 = 5$	$3.1 * 10^{-4}$	$7 * 10^{-9}$		LLS
$FA_{model} = 0.864$	$1.5 * 10^{-4}$	$2 * 10^{-8}$	911/913	PNLS
$SNR_0 = 10$	$4 * 10^{-5}$	$2 * 10^{-9}$		LLS
$FA_{model} = 0.864$	$3.9 * 10^{-5}$	$2 * 10^{-9}$	36/36	PNLS
$SNR_0 = 20$	$7 * 10^{-6}$	10^{-10}		LLS
$FA_{model} = 0.864$	$7 * 10^{-6}$	10^{-10}	0/0	PNLS

MSE: mean squared error; NEG: number of negative eigenvalues λ_3 (smallest eigenvalue) after application of LLS (10,000 simulated tensors); CONV: number of converted positive λ_3 after application of PNLS (starting point from LLS); model parameters from Koay et al. (2006).

presented, see Table 3 for a decoding of the 45 ROI numbers. Such a scheme visualizes a TSBN (i.e. total structural brain network), which is formally a symmetric weighted network with all $n = 45$ ROIs (or nodes) considered and c_{AB} as the edges (Stam and Reijneveld, 2007); see Figs. 3/B–D for examples of connectivity matrices representing TSBNs numerically of a healthy, a MCI converter (MCI-c 21, see Figs. 5/B) and an AD dementia person. For better visualization of the weak connections $\log_{10}(c_{AB})$ is shown as edges, the $n * (n - 1)/2$ edges in the triangle above the matrix-diagonal ($c_{AA} = 0$) represent the information of all pairwise connection strengths of a TSBN, as connectivity matrices are symmetric ($c_{AB} = c_{BA}$).

To construct the structural connectivity network SIBN (i.e. structural intrinsic brain network) of a given IBN, the ROIs are taken from one IBN only, mapping thus an IBN to a corresponding SIBN. As an example, the IBN = DN is indicated by the labels "DN" in Figs. 3/B–D, the corresponding connectivity matrices would have the size $n \times n = 12 \times 12$ presenting all pairwise connections between the ROIs with numbers: 4, 16, 18, 22, 31, 32, 37, 38, 42, 43, 44, and 45.

A SIBN reflects the structural connectivity within a single IBN; but the TSBN includes, beyond structural connections within all 8 IBNs and the hippocampus, additional connections between these IBNs and the hippocampus. Since IBNs-of-interest cover most of the brain's cortex, a TSBN may be interpreted as representative of the IBN-restricted cortical connectome.

Statistical analysis: test statistic and multiplicity correction

Test statistic for univariate analysis

For detecting AD- or MCI-induced changes in a TSBN or SIBN, the edges of the corresponding network are collected in samples. These samples can be defined for a subject, $sample_{subject} = \{c_{AB} | A = 1 \ldots n - 1;\ B = A + 1 \ldots n\}$, or for a group of subjects, $sample_{group} = \{c_{AB(s)} | s = 1 \ldots \text{number of subjects};\ A = 1 \ldots n - 1;\ B = A + 1 \ldots n\}$. Every sample determines a univariate frequency distribution for the edges of a single network or for the edges of a group of networks. See Figs. 4/A–C for examples of probability densities (PDF) and their cumulative distributions (CDF) of group samples. In this presentation the $\log_{10}$ transformation of c_{AB} is applied, improving the resolution along the horizontal axes of the plots.

To test for significant differences between pairs of such distributions (disease-control comparison), we applied a procedure of Brunner and Munzel (2000, 2002). This method is a generalization of the Wilcoxon rank-sum test (restricted to shifted distributions) and is applicable to

Table 3
Regions constituting structural intrinsic brain networks.

ROI	Lobe	Region	IC°/IBN	x	y	z	T	k
1	L/F	Middle frontal gyrus	06, vAN	39	42	33	13.0	216
2	L/F	Dorsolateral PFC	33, dAN	−48	6	33	10.3	161
3	L/F	Supplementary motor cortex	33, dAN	−27	−6	51	8.1	53
4	L/F	Medial PFC	38, aDN	−6	54	18	28.9	4554
5	L/F	Middle frontal gyrus	40, lEN	−45	42	−6	24.6	3977
6	L/F	Superior frontal gyrus	40, lEN	−51	27	15	24.7	3977
7	L/F	Precentral gyrus	43, SMN	−49	3	45	8.2	75
8	R/F	Middle frontal gyrus	06, vAN	36	45	36	11.1	180
9	R/F	Dorsolateral PFC	33, dAN	54	15	24	7.6	98
10	R/F	Frontal eye field	33, dAN	27	3	51	8.7	111
11	R/F	Medial PFC	37, rEN	6	34	37	23.2	4228
12	R/F	Superior frontal gyrus	37, rEN	42	33	30	23.6	4228
13	R/F	Precentral gyrus	43, SMN	47	8	45	9.9	173
14	R/F	Inferior frontal gyrus	06, vAN	57	15	−3	11.9	248
15	R/F	Ventrolateral PFC	37, rEN	37	52	−10	9.65	87
16	R/F	Medial PFC	38, aDN	6	54	18	28.9	4554
17	R/F	Middle frontal gyrus	40, lEN	51	30	30	11.4	120
18	M/F	Medial PFC	38, aDN	0	48	27	28.7	4554
19	M/F	Precentral gyrus	43, SMN	0	12	48	24.1	5002
20	M/F	Anterior cingulate	42, pDN	0	39	9	9.47	85
21	L/T	Inferior temporal gyrus	33, dAN	−51	−60	−9	15.6	537
22	L/T	Inferior temporal gyrus	38, aDN	−63	−12	−15	8.9	135
23	L/T	Middle temporal gyrus	40, lEN	−60	−44	−3	18.4	2379
24	R/T	Inferior temporal gyrus	33, dAN	51	−54	−9	19.9	914
25	R/T	Middle temporal gyrus	37, rEN	66	−39	−3	12.5	2322
26	L/P	Inferior parietal lobe	06, vAN	−63	−33	27	19.3	2338
27	L/P	Inferior parietal lobe	33, dAN	−45	−36	48	19.6	1849
28	L/P	Superior parietal lobe	33, dAN	−21	−63	54	16.7	1849
29	L/P	Inferior parietal lobe	37, rEN	−51	−54	51	13.9	450
30	L/P	Inferior parietal lobe	40, lEN	−39	−60	42	18.6	2379
31	L/P	Inferior parietal lobe	42, pDN	−39	−69	39	14.8	505
32	L/P	Posterior cingulate	42, pDN	−6	−45	33	23.0	2857
33	R/P	Inferior parietal lobe	06, vAN	60	−33	33	21.8	2005
34	R/P	Inferior parietal lobe	33, dAN	39	−36	45	18.4	2067
35	R/P	Superior parietal lobe	33, dAN	51	−33	51	18.1	2067
36	R/P	Inferior parietal lobe	37, rEN	54	−51	45	26.1	2322
37	R/P	Inferior parietal lobe	42, pDN	45	−66	42	12.2	431
38	R/P	Posterior cingulate	42, pDN	6	−54	21	30.9	2857
39	M/P	Cingulate gyrus	06, vAN	0	−48	51	13.2	1309
40	L/O	Visual area 1	08, pVN	−12	−81	0	18.0	3081
41	R/O	Visual area 1	08, pVN	6	−81	3	16.4	3081
42	L/T	Anterior left hippocampus	–					
43	L/T	Posterior left hippocampus	–					
44	R/T	Anterior right hippocampus	–					
45	R/T	Posterior right hippocampus	–					

a pair of arbitrarily shaped distributions; ties and different sample sizes are also admissible.

This procedure quantifies in our context whether the edges of one sample have a tendency to be smaller than those in the comparative sample, testing the Null hypothesis H^B_0 (edge samples for disease and healthy control are tendentiously equal) versus the alternative hypothesis (disease reduces edges). Technically, a rank statistic T_B is calculated from the individual elements (edges) of the two samples to compare, it is defined by

$$T_B = \sqrt{n_1 n_2/(n_1+n_2)} * (R_2 - R_1)/\sigma_B$$

where n_i = size of sample i, $i = 1,2$; R_i = mean (combined-sample) rank of individual edges from sample i, and σ_B^2 = rank based combined variance (for an algorithm to calculate T_B see (Neuhäuser and Ruxton, 2009)). Permutation resampling is recommended (Neubert and Brunner, 2006) to achieve H^B_0-distributions of T_B, for large samples the H^B_0-distribution can be approximated by the standard Normal N(0,1). Brunner's method overcomes limitations of elder methods, which are less flexible, see (Neuhäuser and Ruxton, 2009; Rorden et al., 2007) for a comparison with standard methods such as two-sample t-test. T_B is not modified by a $\log_{10}$ transformation of the sample elements, as their order remains unchanged.

To evaluate our statistical approach based on Brunner's procedure, we performed a second analysis based on the two-sample Kolmogorov–Smirnov (K–S) test (Conover, 1980). This test quantifies the difference of two samples by the maximum difference of their CDFs, see Fig. 4. The Kolmogorov–Smirnov test statistic is also not modified by a $\log_{10}$ transformation (Press et al., 1992).

Both tests measure the tendency that elements in one sample are smaller than the elements of the second sample. The K–S test relies on the standard H_0: $CDF_X = CDF_Y$, where X and Y denote the random variables of sample 1 and sample 2 (Conover, 1980). Note, that Brunner's test applies a different H^B_0 which involves the relative effect p, introduced by Mann and Whitney (1947). The relative effect p is a functional of the two samples measuring the shifts of their elements (simplifying one might say, p plays for random samples a similar role like e.g. the correlation coefficient for time series); it is defined by $p = \text{Prob}(X < Y) + 0.5\ \text{Prob}(X = Y)$, in other words: if one randomly selects X from sample 1 and Y from sample 2, Prob(X < Y) denotes the probability that X < Y and Prob(X = Y) denotes the probability for X = Y. If $p > 0.5$ then the observations X tend to be smaller than the Y's, for $p < 0.5$ vice versa, for $p = 0.5$ they are (stochastically) tendentiously equal. The larger $|p - 0.5|$, the stronger the deviations between the samples or their distributions. The Null hypothesis for Brunner's test is H^B_0: $p = 0.5$, one can show that the standard H_0 implies H^B_0, but H^B_0 is more general including also the Behrens–Fisher problem. The test statistic T_B can be rewritten as $T_B = \sqrt{n_1 + n_2}(p-0.5)/\sigma_B$ (Brunner and Munzel, 2000, 2002).

Examples for the relative effect p, comparing two Bernoulli PDFs, are presented in Fig. 4/D. The Bernoulli distributions $B_1(X)$ (green color) and $B_2(Y)$ (red color) are defined for X,Y = {0 or 1}. For $p = 0.55/0.45$ the corresponding distribution pairs are shown; for the probabilities $q_1 = \text{Prob}(X = 1)$ and $q_2 = \text{Prob}(Y = 1)$, p can be calculated analytically, $p = 1/2 - 1/2 * (q_1 - q_2)$, see the diagonal line for all combinations of q_1 and q_2.

Multiple testing procedures

As the reduction of structural connectivity strengths in AD is tested for several sample pairs, multiple pairwise comparisons must be performed (Westfall and Young, 1993). Since connections within a SIBN or TSBN might be correlated, we incorporated T_B into a multiple testing scheme with minimal assumptions, which concedes correlations within samples (Westfall and Troendle, 2008). This statistical context was used to calculate raw and multiplicity adjusted P-values (P_{raw}, P_{ad}) for the comparisons. P_{raw} is the usual P-value of a single test as described in the Test statistic for univariate analysis section, for $P_{raw} \le \alpha$ the "comparisonwise" type I error rate (false positives) is controlled at significance level α e.g. $\alpha = 5\%$. P_{ad} includes by construction an adjustment to reduce false positives caused by the multiplicity of all comparisons within the testing family; for $P_{ad} \le \alpha$ it controls the family wise error rate (FWER) strongly at level α; that means: $\max_{I \subseteq M} \text{Prob}\left(V > 0 \middle| \bigcap_{i \in I} H_{0i}\right) \le \alpha$, where the maximum is taken for all configurations $I \subseteq M$, and for V = number of false positives, M = {1…m} for m Null hypotheses in total, and H_{0i} denotes a specific Null hypothesis i (Bretz et al., 2011; Westfall and Young, 1993). The simplest (often too conservative) strong FWER adjustment is due to Bonferroni, with P_{ad} = (number of tests) * P_{raw}, indicating that the number of testing-hypotheses (|testing-family|) is a critical parameter. As our number of hypotheses concerning structural connectivity is moderate (|testing-family| = 46, see the Design of statistics section), FWER is more convenient than e.g. the more liberal false discovery rate (FDR), which could increase the number of significant rejections, but also the risk of false positives. Thus, the design of our structural analysis aims at the detection of connectivity effects with strong statistical evidence.

Results

Functional connectivity of IBNs: selective disruptions in the default mode network of patients

Fig. 1 presents spatial maps of independent components (ICs) derived from ICA of rs-fMRI data (color maps show t-values from one-sample t-tests). ICs reflect IBNs of interest (i.e. pDN, aDN, dAN, vAN, lEN, rEN, SMN, and VN), which were identified by independent raters (A.W., C.S.) with 100% inter-rater consistency. Furthermore, identified IBNs match previous findings (e.g. Agosta et al., 2012; Sorg et al., 2007). Group comparisons framed by ANOVA of spatial IC maps reveal only for the pDN significant group differences in the posterior parietal cortex. Post-hoc two-sample t-tests demonstrate increasing reduction of network functional connectivity in patients with MCI and AD compared with healthy controls in the posterior parietal cortex (Fig. 1/H; MCI < controls, $p < 0.05$ FDR adjusted; clusters in the posterior cingulate cortex with [peak (−12,−54,33)/t-value 5.85/cluster size 136], the middle cingulate gyrus [(27,−6,33)/4.68/43], and the middle occipital gyrus [(−27,−84,9)/4.66/44)]).

To evaluate the potential impact of atrophy on patients' intrinsic functional connectivity changes within the pDN, we performed additional VBM analysis of structural MRI data. In line with previous studies (for brief review see Ewers et al., 2011), we found increasing atrophy in medial and lateral temporoparietal areas of patients (ANOVA, $p < 0.05$ FWE-corrected, data not shown). Atrophy was not overlapping with disrupted functional connectivity within the pDN. Furthermore, when including individual VBM-volumes of the pDN as additional covariate in the ANOVA of pDN functional connectivity, the observed pattern of reduced connectivity was not changed. This independence of pDN connectivity changes on atrophy indicates the functional nature of pDN connectivity alterations in patients.

IBN based structural connectivity: connectivity matrices and corresponding edge distributions of group samples

Figs. 2 and 3 present results of tractography and its combination with IBN-ROIs to construct connectivity matrices of SIBNs (and TSBNs). The quality of TEND tractography is exemplified in Figs. 2/A−C, where fibers of the corpus callosum are presented. To calculate fiber connectivity, approximately $1.3 * 10^6$ white matter voxels (1 mm^3) are used in

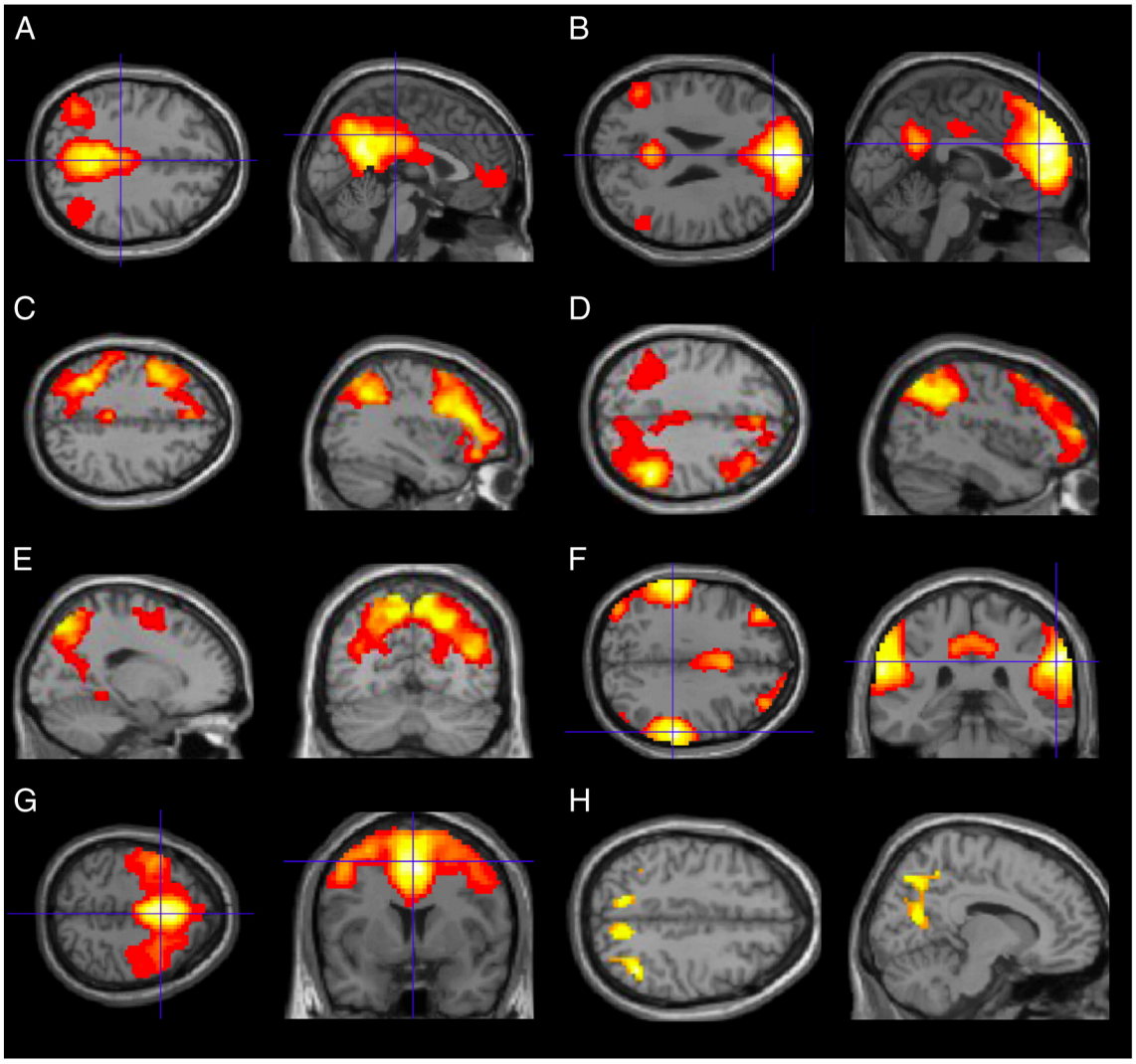

Fig. 1. Intrinsic brain networks and group comparisons. (A–G) Intrinsic brain networks (IBNs), collapsed over all groups: IBNs were derived from spatial maps of an independent component analysis of resting-state fMRI data, the IBNs are used for the definition of seed regions for fiber tracking. Restricted to IBNs of interest, color maps indicate t-values from one-sample t-tests on spatial maps of independent components including all participants (red to yellow 1.8 to 9.2), thresholded at $p < 0.05$, FDR-adjusted, and rendered on a standard brain in MNI space. For exact t-values of cluster peaks, cluster size, and regional labeling see Table 3. (A) refers to the posterior default mode network (peak (6/-54/21)), (B) the anterior default mode network (−6/54/18), (C) a left-lateralized executive network (−51/27/15), (D) a right-lateralized executive network (54/−51/45), (E) a dorsal attention network (51/−54/−9), (F) a ventral attention network (60/−33/33), and (G) the sensorimotor network (0/12/48). (H) group comparisons: Concerning comparisons across subjects, for each IBN individual maps were entered into voxel-wise analysis of variance (ANOVA). Only maps of the posterior default mode network were significantly different across groups. Panel (H) shows voxels of the posterior default mode, for which patients with MCI had reduced within-network functional connectivity compared with healthy controls (post-hoc two-sample t-test on spatial independent component map of the pDN, $pFDR < 0.05$, colors indicate t-values, red to yellow 1.7 to 6.9).

every brain for brute force seeding. Fig. 2/D shows a subset of such fibers connecting IBN-ROIs of the DN. The pattern of tracks, which connect the medial prefrontal cortex ROIs (numbers 4, 18 in Fig. 2/D) with the posterior cingulate cortex (numbers 32, 38), is similar to findings of Greicius et al. (2009). Fig. 3/A presents the spatial network of a TSBN, see Table 3 for decoding the ROI numbers. In Figs. 3/B–D TSBN connectivity matrices for a healthy, a MCI and an AD subject are presented; the connections (edges of the corresponding structural networks) are $\log_{10}(c_{AB})$, where c_{AB} = "connection probability". Reductions of connectivity strengths under disease are clearly visible.

Fig. 4 presents edge distributions of some empirical group sample networks. For $\log_{10}(c_{AB})$ we show the probability density (PDF) and cumulative distribution (CDF) of control, MCI and AD groups for the SIBNs of DN and dAN, and for the TSBN (Figs. 4/A–C). In all three panels a clear tendency of reduction for the connection probability c_{AB} for patients can be observed. For the DN, connectivity of patients with MCI is less reduced than that of patients with AD, for the dAN vice versa, for TSBN patients with MCI and AD show nearly identical reductions.

Group–group comparisons: selective and progressive disruptions in the structural connectivity of IBNs in Alzheimer's disease

(i) *Scores of test statistic T_B*: In Fig. 5/A, blue points show Brunner's test statistic T_B quantifying the reduction of connectivity in the patient sample compared to the control sample (one sided testing was performed). The corresponding labeling at the bottom line has to be interpreted in the following way: e.g. in the case of the first column (TSBN, MCI), group sample of TSBNs for MCI subjects is compared to group sample of TSBNs for controls. For the approximate Null distribution N(0,1), T_B indicates partly stronger reductions for TSBNs than for DNs and dAN, which may be an effect of its major sample size (size-TSBN ~ 20.000, size-DN ~ 1.400, size-dAN ~ 800), as testing power increases with sample size.

(ii) *P-values*: For H^B_0, we calculated the T_B distributions by permutation-based resampling for 10^5 permutations and derived corresponding raw P-values (Fig. 5/A, yellow points: P_{raw}) for a

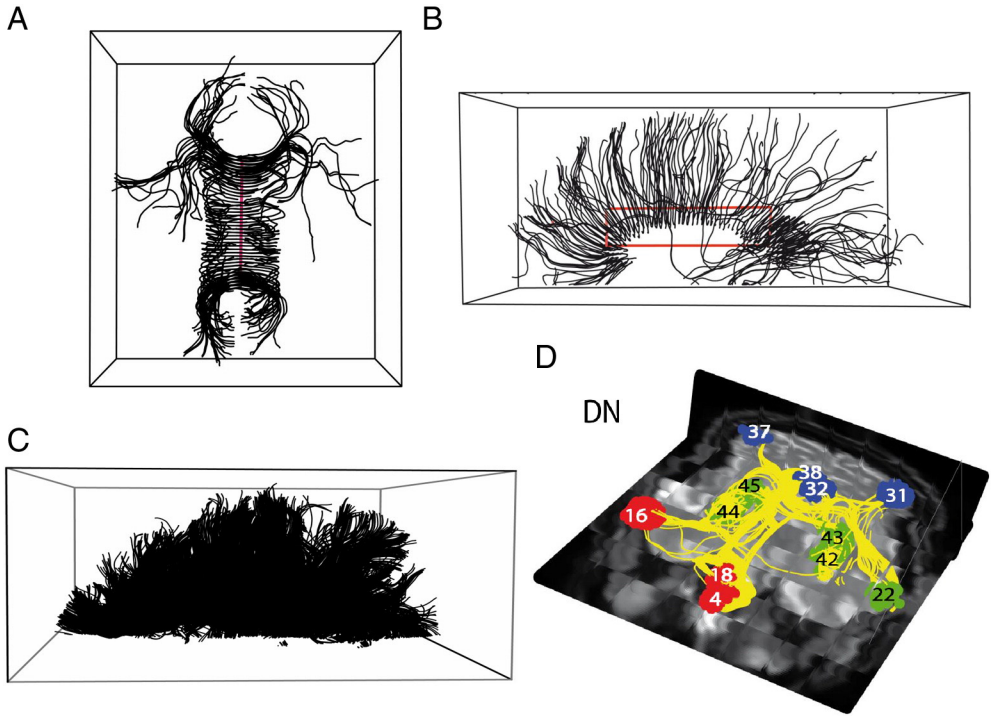

Fig. 2. Illustrating fiber tracking. Panel A), axial view of corpus callosum fibers calculated with TEND tractography, selected seed points from red line. Panel B), sagittal view of fibers from panel A); red box indicates brute force seed points for fibers of panel C) shown also in sagittal view. Panel D), fibers (yellow) connecting the IBN-ROIs of the default mode network (DN); ROI coloring and labeling is the same as the spatial total network shown in Fig. 3/A, see Table 3 for decoding.

one sided antithesis (c_{AB} values are changed to smaller values by MCI or AD compared to the control). P_{raw} values were then adjusted for multiplicity by Westfall's method (red points: P_{ad}). Levels of significance, $\alpha = 5\%$, and of marginal significance, $\alpha = 10\%$, for the P-values are indicated by horizontal lines. The results indicate significant (5%) decreases of connectivity strength for TSBN and DN of patients with AD and MCI as well as for the dAN of patients with MCI. To check if simpler procedures can cope with Brunner's/Westfall's method, Bonferroni adjusted P-values based on (one sided) Kolmogorov–Smirnov tests (gray points: $P_{ad\ KS}$) were also calculated. Both adjusted P-values agree qualitatively, however the connectivity reduction of dAN/MCI patients is no more significant (5%) for $P_{ad\ KS}$.

Subject–group comparisons: disrupted structural connectivity separates MCI patients converting to AD dementia from non-converters

We repeated the procedure for the TSBNs in the Group–group comparisons: selective and progressive disruptions in the structural connectivity of IBNs in Alzheimer disease section with the modification that the patient group samples were replaced by samples of individual MCI patients. In Fig. 5/B the results are shown for MCI converters (MCI-c) and in Fig. 5/C for non-converters (MCI-nc). Patients are labeled by numbers at the bottom line; coloring for T_B, P_{raw}, P_{ad} and $P_{ad\ KS}$ is the same in Fig. 5/A.

As in subject-based samples the collective variance component caused by subject variation is missing, exchangeability with the healthy control group sample, which is a necessary condition for permutation resampling (Good, 2004), may be not fulfilled. Therefore a further evaluation, based on N(0,1) and the standard Bonferroni correction (|testing-family| = 46, see the Design of statistics section) is performed, see $P_{ad\ N(0,1)}$ (green points). The two sets of adjusted P-values are quite similar indicating a solid stability of our statistical evaluation. The corresponding $P_{ad\ KS}$ values, agree qualitatively with P_{ad} like in the group–group comparisons, and the number of significant and marginally significant reductions is again somewhat smaller.

In Fig. 5/B we find 7 converters with $P_{ad} < 5\%$ and 8 converters with $P_{ad} < 10\%$; these correspond to a sensitivity of 0.54 and 0.62. For the non-converters in Fig. 5/C we find for $P_{ad} > 5\%$ 14 non-converters and for $P_{ad} > 10\%$ 13 non-converters; the corresponding specificities are 0.93 and 0.87. Sensitivity and specificity are interpreted for a binary classification of the clinical MCI converters and non-converters. As indicator for converters the significant reduction of connectivity compared to a control group is applied.

Analysis with a second connectivity strength

A second connectivity strength was introduced in the Tractography and connectivity strength section to control the model dependence of our results. The reanalysis with this second measure gives the following results: Very similar patterns of the distributions, as shown in Fig. 4, are achieved for c_{AB} = "connection density". Also the group–group and subject–group results, plotted in Fig. 5, are reproduced with minor modifications.

Discussion

In line with our hypotheses, we found structural connectivity of IBNs selectively and for DN progressively (increasing with severity) disrupted in AD dementia and MCI with most significant changes in the DN. This result extends previous DTI-findings of widespread and progressive white matter disruptions in AD. Secondly, disrupted structural connectivity corresponded with impaired functional connectivity in the DN of patients. This correspondence suggests that reduced functional connectivity of intrinsic networks can reflect impaired structural connectivity in AD. Finally, at single subject level, structural connectivity across nodes of all intrinsic networks was reduced specifically in MCI patients, who converted to AD within 3 years. This last finding indicates the sensitivity of structural connectivity for AD. To achieve these results, we introduced a novel

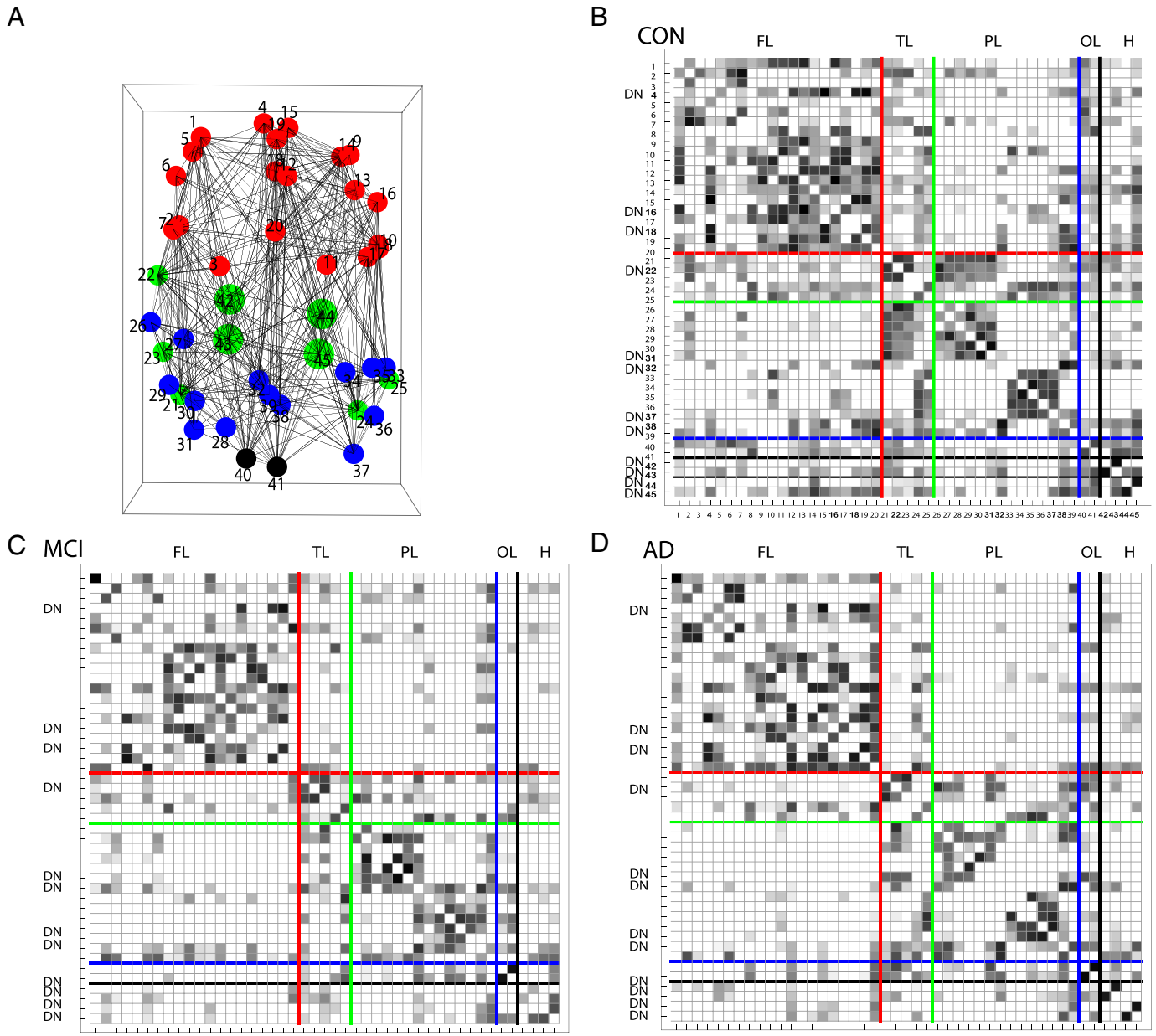

Fig. 3. Structural connectivity, c_{AB} = connection probability. Panel A presents the total spatial network (TSBN) in a 3 dimensional perspective. Panels B–D) present connectivity matrices of log10(c_{AB}) for the TSBN of a healthy (B), MCI (C) and AD (D) subject; ROI numbering is consistent in panels A–D), see Table 3 for anatomical decoding. The DN ROIs in the connectivity matrices of panels B–D) are emphasized (left column), the lobes are separated on top of the matrices (red and FL = frontal lobe, green and TL = temporal lobe, blue and PL = parietal lobe, black and OL = occipital lobe, H = hippocampus); connectivity strength increases with darkening of matrix-pixels, the three matrices are comparable due to convenient normalization.

approach to analyze brain connectivity matrices by the use of non-parametric statistical methods including procedures for multiple testing. This approach relies basically on the mathematical possibility to analyze univariate frequency distributions of network edges for across-subject comparisons. In the following, we discuss these findings in detail.

Disrupted structural connectivity of intrinsic functional brain networks in AD

Selective and progressive impact of AD on IBN structural connectivity

In patients with AD dementia and MCI, we found selectively (in TSBNs and in attention networks) and progressively in the DN disrupted structural connectivity (Fig. 5/A). Results were independent of age, gender, and education, since groups were not different for these parameters (Table 1). Several previous DTI-studies in AD and MCI support this result by demonstrating widespread and progressively aberrant structural connectivity in patients (for example Lo et al., 2010; Shao et al., 2012; for review Sexton et al., 2011); since most of these studies performed region-based approaches (e.g. whole brain voxelwise comparisons for white matter properties such as fractional anisotropy or brain atlas-based tractography approaches), these studies were not able to provide direct evidence for structural connectivity disruptions in IBNs. In contrast, the current study determined explicitly IBNs by the use of independent rs-fMRI analysis (Fig. 1), which allowed for explicit network-based findings.

Reduced connectivity strength was more prominent in the DN than in attention networks (Fig. 5/A). Furthermore, disrupted connectivity in the DN was more prominent in patients with AD than in those with MCI, suggesting increasing alterations of DN structural

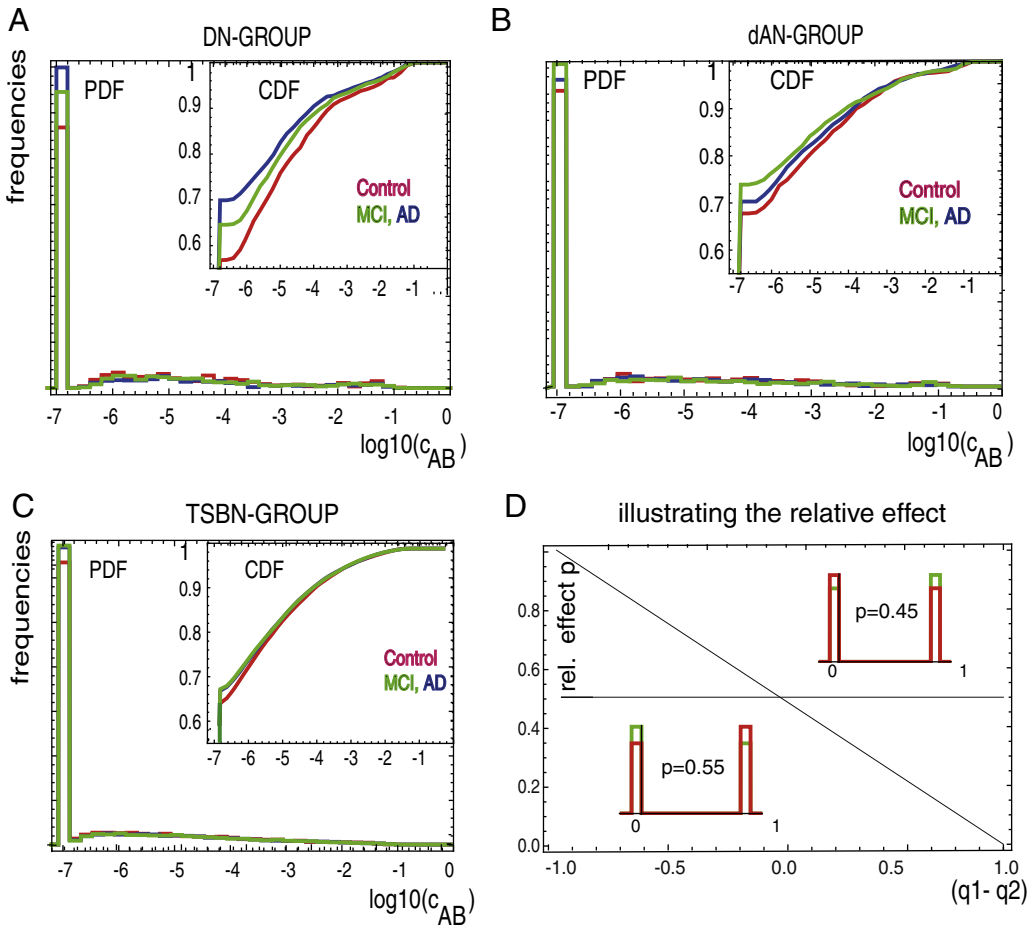

Fig. 4. Group samples for different networks, c_{AB} = connection probability. Panels A, B, and C show probability densities (PDF) and cumulative distributions (CDF) of log10(c_{AB}) for group samples of different networks (red: healthy control, green: MCI, blue: AD; $c_{AB} = 0$ is mapped to $c_{AB} = 10^{-7}$). Panel A) refers to the default mode network (DN), panel B) to the dorsal attention network (dAN) and panel C) to the total structural network TSBN. In all panels a clear tendency for lowering c_{AB} values under disease can be observed. Panel D) illustrates the relative effect p by the comparison of two Bernoulli distributions B1(X) (green) and B2(Y) (red) for $p = 0.55$ and $p = 0.45$; for tendency X smaller Y, $p > 0.5$, for X larger Y, $p < 0.5$. The diagonal line gives the functional $p = p(q_1 - q_2)$, where $q_1 = \text{Prob}(X = 1)$ and $q_2 = \text{Prob}(Y = 1)$.

connectivity in AD (Fig. 5/A). Disrupted structural connectivity in lateral frontoparietal attention networks was found in the dAN of patients with MCI; structural connectivity reductions in the vAN of patients with dementia did not (completely) survive corrections for multiple comparisons (Fig. 5/A). This pattern of consistent changes in the DN but less consistent ones in the lateral attention networks is in line with other findings in patients with early AD, which are based on brain modalities distinct from structural connectivity (such as glucose metabolism or functional connectivity) (Fouquet et al., 2009; Sorg et al., 2009). For example, recent fMRI studies demonstrated impaired functional and effective connectivity in lateral frontoparietal attention networks in MCI, prodromal and dementia AD (Agosta et al., 2012; Li et al., in press; Neufang et al., 2011; Sorg et al., 2007); but these functional changes are not perfectly consistent across studies concerning time of onset and network specificity (Agosta et al., 2012; Drzezga et al., 2011; Li et al., in press; Sorg et al., 2007, 2009). In contrast to this inconsistency, fMRI studies in persons at-risk for AD, with AD-MCI or AD dementia found robust progressive disruptions of DN's functional connectivity (Drzezga et al., 2011; Greicius et al., 2004; Mormino et al., 2011; Sorg et al., 2007, 2009). It seems that the DN is more consistently altered in early AD than lateral attention networks, in other words AD seems to affect primarily the DN. How may be this specificity explained? The DN has elevated levels of intrinsic activity compared with other networks (Buckner et al., 2009); furthermore, increased levels of intrinsic activity are related with an increased vulnerability for amyloid pathology (for brief review Sheline and Raichle, 2013); therefore, it has been suggested that lifelong increased intrinsic activity predisposes the DN for amyloid pathology, which in turn is the initiating event in AD pathogenesis (amyloid cascade hypothesis of AD) (Blennow et al., 2006). Our result of selective and progressive disruptions of DN structural connectivity strengthens this view of AD (Buckner et al., 2009; Pievani et al., 2011). Future studies are needed to analyze explicitly the link between structural connectivity changes in intrinsic networks particularly the DN and the pattern of amyloid pathology in patients.

Correspondence between disrupted functional and structural connectivity in IBN

Additionally, we found selective and progressive functional connectivity reductions in the DN (Fig. 1/H). This result (when restricted to MCI patients) replicates a previous finding of our group in an independent sample of patients (Sorg et al., 2007; for AD dementia, see Agosta et al., 2012). Progressively reduced functional connectivity in the DN perfectly corresponds with progressively reduced structural connectivity in the DN (Figs. 1/H, 5/A). This correspondence of functional and structural connectivity disruptions suggests that disrupted functional connectivity can reflect, at least partly, impaired structural connectivity. Previous studies in healthy controls support this interpretation by demonstrating partial correspondence between

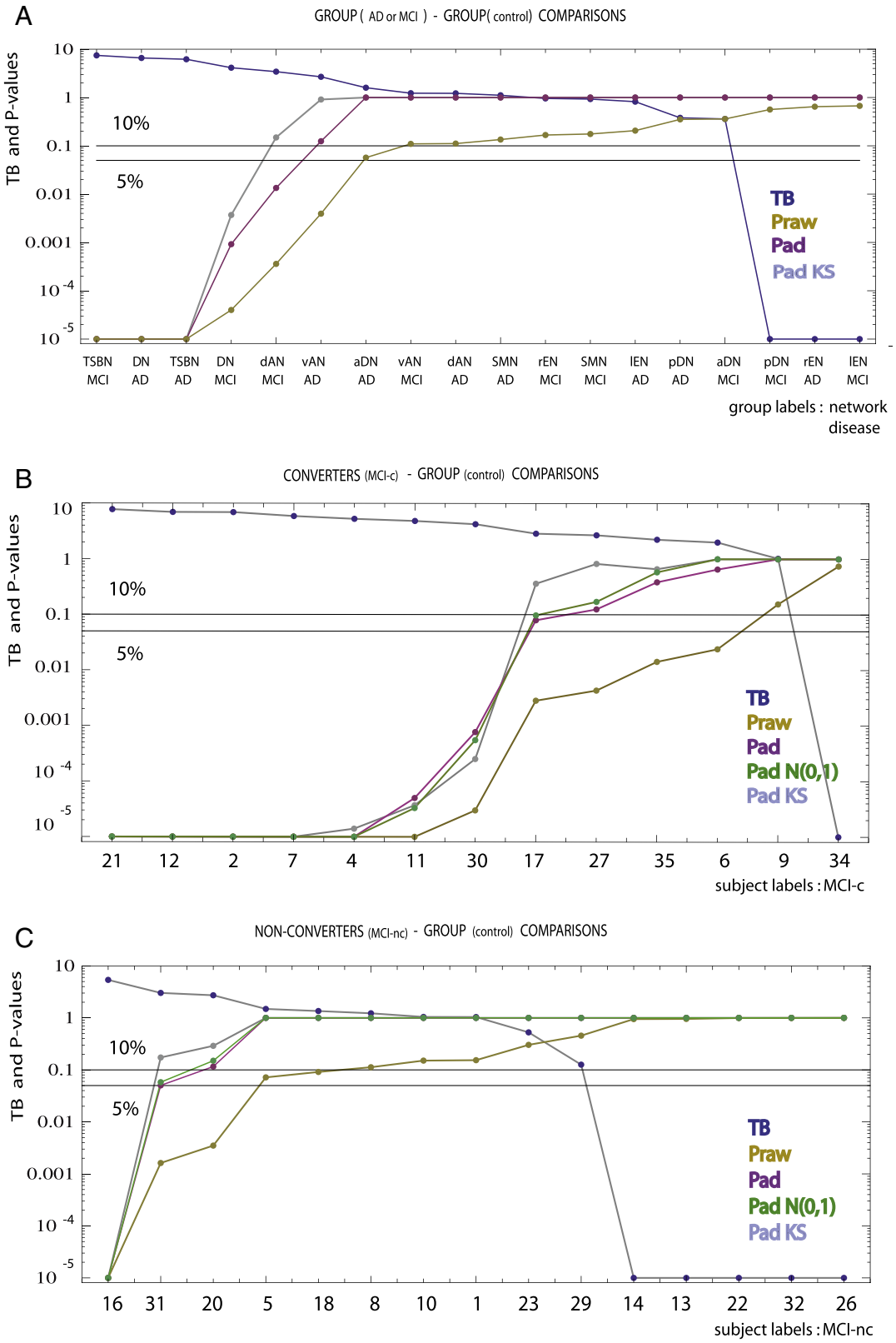

Fig. 5. Comparing structural connectivity for intrinsic networks (SIBN) and the total network (TSBN), c_{AB} = connection probability. Panels A–C) present Brunner's test statistics TB (blue), corresponding P-values for pair-wise comparisons and two lines which give the levels of significance $\alpha = 5\%$ and of marginal significance $\alpha = 10\%$. Yellow points — P_{raw} values calculated by Brunner's method, red points — P_{ad} calculated by Westfall's method applied to P_{raw}, green points — P_{ad} N(0,1) calculated by Brunner's Null distribution N(0,1) and Bonferroni adjustment, gray points — P_{ad} KS based on Kolmogorov–Smirnov tests with Bonferroni adjustment. Panel A) presents group–group comparisons of patients versus healthy controls; labels at bottom line indicate the networks TSBN or SIBN and the patient group (MCI, AD) which are compared with the corresponding networks of the control group. Panel B) presents results for subject–group comparisons of converting patients (MCI-c) versus healthy controls, the network is in all cases TSBN; numbers refer to individual MCI-c patients converting to AD within 3 years. Panel C) presents results for non-converting patients (MCI-nc) versus healthy controls, else like B).

structural and functional connectivity in IBNs (Hagmann et al., 2008; Greicius et al., 2009; van den Heuvel et al., 2009). Furthermore, Zhou et al. (2008) reported the tendency for correspondingly reduced functional and structural connectivity between the hippocampus and posterior parietal cortex in patients with AD dementia; both areas are critical regions of the DN covered by our DN definition (see Figs. 1 and 3). To explore whether observed DN functional connectivity changes of asymptomatic persons at risk for AD are also associated with structural connectivity changes or reflect "pure" functional alterations, future studies are necessary.

Classification of clinical MCI converters and non-converters

Even at single subject level selected MCI patients had significantly reduced connectivity strength for the total network TSBN. Clinically, 13 of a total of 28 MCI patients converted to AD within 3 years, see Fig. 5/B; the 15 non-converters are presented in Fig. 5/C. Sensitivity for converters equals 0.54 for significant P_{ad} and 0.62 for marginally significant P_{ad}; specificity for non-converters is correspondingly 0.93 and 0.87. This is in line with previous results, where individual AD-converters were successfully classified from healthy controls due to changes in fiber-based metrics (Shao et al., 2012). These results were achieved by non-inferential methods from information theory, using as classifiers the support vector machine, the k-nearest neighbor and naive Bayes.

To test dependence of our classification results on sample size, we reduced the size of the control group samples by factors 1/2, 1/4 and 1/8 and recalculated sensitivity and specificity for $P_{ad} < 5\%$ and $<10\%$. Both measures were nearly unchanged for different sample sizes, indicating no essential loss of classification quality for smaller control groups or less experimental expenditure. Also the ratios between the numbers of significant (or marginally significant) group–group differences and all group–group comparisons as shown in Fig. 5/A were calculated. Interestingly, this ratio showed clear monotonous reduction with decreased sample sizes. This indicates that for the group–group comparisons data reduction is not admissible.

In summary we conclude, that fiber-based connectivity may allow for identifying prodromal AD at single subject level; in other words, total structural connectivity networks may have the potential for an imaging-based biomarker separating early AD from healthy aging. Concerning this last point, studies are necessary to explore this biomarker potential, focusing on test–retest reliability of T1-, DTI- and rs-fMRI-based metrics across time, analysis protocols, different scanners or scanner elements. For healthy subjects Basset et al. (2011) and Huang et al. (2012) found reproducibility for these MRI modalities; but also studies for patients with MCI or early AD might be helpful.

Methodological issues

Restrictions and univariate analysis

Our multimodal imaging protocol including diffusion, T1, and resting-state functional MRI is of short scanning time due to potential compliance problems of elder patients. This implies particularly for the DWIs rather large voxel sizes to increase signal to noise ratios, as measurement replications must be avoided; in addition only a moderate number ($n = 15$) of diffusion gradients can be applied, though connectivity could be increased by more gradients (Deligianni et al., 2012). Distortion corrections are performed by application of the FSL software, but residual distortions may still exist in the DWIs, which are finally fitted to the standard tensor model (Basser and Jones, 2002). It was shown by an analysis without application of FSL that strong distortions (caused by head motion and eddy currents) would have a severe impact on the results shown in Fig. 5; e.g. if the distortion correction is discarded in the DWIs of MCI and AD patients, no group–group comparison of Fig. 5/A has adjusted P values below 5%. On the other hand, it may be possible that more advanced distortion corrections than that applied in FSL could reveal additional significant differences.

All these present limitations restrict the accuracy of tractography: crossing or branching fibers cannot be modeled by the standard tensor model (see e.g. Hahn et al. (2013) for alternatives), big voxels tend to linearize the fiber courses by averaging, low direction DWIs and residual distortions may reduce connectivity. Due to these limitations, we restrict our analysis of fiber based connectivity to univariate edge distributions across nodes of the SIBNs or TSBNs. Edge distributions could be more robust against smaller fractions of wrong or missing connections than e.g. more differentiating network parameters, like clustering coefficients or path lengths (Stam and Reijneveld, 2007).

Design of statistics

Such univariate edge distributions deviate strongly from Gaussian distributions and need consequently a flexible nonparametric statistics, like Brunner's test statistic. It was used together with a procedure correcting for multiple testing, to achieve strong control for the FWER. As family for the adjusted P-values in Figs. 5/A–C, we regard all 46 group–group and subject–group comparisons together, in line with criteria (i–iii) in Westfall and Young (1993, p.220): (i) The research questions underlying different tests form a natural and coherent unit, e.g. if they all result from a single experiment (note, that the control group is involved in every test); (ii) tests have to be considered simultaneously for a summary; and (iii) it is considered a priori probable that many or all members of the family of Null hypotheses are in fact true. These conditions fit the tests presented in Fig. 5/A–C if we regard the IBN-ROIs as given base for structural statistical analysis. One might speculate, to include additional hypotheses about e.g. the internal connections within the DN, or between DN and other IBNs in this study. However, such extensions would enlarge the testing-family and consequently all adjusted P-values. As our goal was to find effects with strong evidence, we did not include more hypotheses. The findings of this study are based on the Brunner's/Westfall's approach (Brunner and Munzel, 2000; Westfall and Troendle, 2008); a correspondent Kolmogorov–Smirnov/Bonferroni approach (Conover, 1980) gave similar results, however fewer significant effects.

Measures of connectivity strength

As no best choice for a measure of connectivity strength is available, a particular dependence on a specific definition would restrict the relevance of our findings. Therefore a reanalysis with a second measure, namely c_{AB} = "connection density", was performed. We got close consistency between both results. This independence on the normalization of c_{AB} might be understood by the distributions in Figs. 4/A–C. Concerning PDFs, disease-induced changes appear to be expressed predominantly by an increase of the $c_{AB} = 0$ connections (mapped to 10^{-7} in Figs. 4/A–C); for the zero connections, however, normalization does not matter. The distribution patterns in Figs. 4/A–C and the matrices in Figs. 3/B–D indicate additionally that AD and MCI influence mainly the weak fiber connections by reducing them to zero. In our study, we focused on tractography-scores in contrast to FA- or MD-scores, which are discussed in Sexton et al. (2011). This focus is in line with Bozzali et al. (2011), who showed that tractography-based scores appear to be more sensitive for AD's effects than FA-scores; in their study, observed FA-differences lost significance after multiplicity adjustment.

Conclusion

Current results provide evidence for selective and progressive disruptions of IBNs' structural connectivity in AD, which correspond with changes of IBN's functional connectivity. Applying a flexible nonparametric statistic and a recent derivation of multiplicity

adjusted P-values on edge distributions of structural connectivity networks, our method detects disruptions with strong statistical evidence and with high power. The method is applicable to any symmetric weighted network.

Acknowledgment

We thank Prof. E. Brunner for his helpful comments on the use of his T_B statistics and the unknown reviewers for their substantial, constructive suggestions. A.M.W. is supported by the German Federal Ministry of Education and Research (BMBF) grant 01EV0710 and C.S. is supported by the Kommission für Klinische Forschung of the university hospital Klinikum Rechts der Isar grant 8765162 and (BMBF) grant 01ER0803.

Conflict of interest

No competing financial interest exists.

References

Agosta, F., Pievani, M., Geroldi, C., Copetti, M., Frisoni, G.B., Filippi, M., 2012. Resting state fMRI in Alzheimer's disease: beyond the default mode network. Neurobiol. Aging 33 (8), 1564–1578.

Arsigny, V., Fillard, P., Pennec, X., Ayache, N., 2006. Log-Euclidean metrics for fast and simple calculus on diffusion tensors. Magn. Reson. Med. 56, 411–421.

Basser, P.J., Jones, D.K., 2002. Diffusion-tensor MRI: theory, experimental design and data analysis — a technical review. NMR Biomed. 15, 456–467.

Basset, D.S., Brown, J.A., Deshpande, V., Carlson, J.M., Grafton, S.T., 2011. Conserved and variable architecture of human white matter connectivity. NeuroImage 54, 1262–1279.

Bateman, R.J., Xiong, C., Benzinger, T.L., Fagan, A.M., Goate, A., Fox, N.C., Marcus, D.S., Cairns, N.J., Xie, X., Blazey, T.M., Holtzman, D.M., Santacruz, A., Buckles, V., Oliver, A., Moulder, K., Aisen, P.S., Ghetti, B., Klunk, W.E., McDade, E., Martins, R.N., Masters, C.L., Mayeux, R., Ringman, J.M., Rossor, M.N., Schofield, P.R., Sperling, R.A., Salloway, S., Morris, J.C., 2012. Clinical and biomarker changes in dominantly inherited Alzheimer's disease. N. Engl. J. Med. 367 (9), 795–804.

Blennow, K., de Leon, M.J., Zetterberg, H., 2006. Alzheimer's disease. Lancet 368, 387–403.

Bozzali, M., Parker, G.J., Serra, L., Embleton, K., Gili, T., Perri, R., Caltagirone, C., Cercignani, M., 2011. Anatomical connectivity mapping: a new tool to assess brain disconnection in Alzheimer's disease. NeuroImage 54, 2045–2051.

Braak, H., Braak, E., 1991. Neuropathological stageing of Alzheimer-related changes. Acta Neuropathol. (Berl.) 82, 239–259.

Bretz, F., Hothorn, T., Westfall, P., 2011. Multiple Comparisons Using R. Chapman & Hall/CRC.

Brunner, E., Munzel, U., 2000. Nonparametric Behrens–Fisher problem: asymptotic theory and a small-sample approximation. Biom. J. 42 (1), 17–25.

Brunner, E., Munzel, U., 2002. Nicht-parametrische Datenanalyse. Springer-Berlin, Heidelberg, New York.

Buckner, R.L., Andrews-Hanna, J.R., Schacter, D.L., 2008. The brain's default network: anatomy, function, and relevance to disease. Ann. N. Y. Acad. Sci. 1124, 1–38.

Buckner, R.L., Sepulcre, J., Talukdar, T., Krienen, F.M., Liu, H., Hedden, T., Andrews-Hanna, J.R., Sperling, R.A., Johnson, K.A., 2009. Cortical hubs revealed by intrinsic functional connectivity: mapping, assessment of stability, and relation to Alzheimer's disease. J. Neurosci. 29, 1860–1873.

Calhoun, V.D., Adali, T., Pearlson, G.D., Pekar, J.J., 2001. A method for making group inferences from functional MRI data using independent component analysis. Hum. Brain Mapp. 14, 140–151.

Conover, W.J., 1980. Practical nonparametric statistics. Wiley Series in Probability and Statistics.

Deligianni, F., Robinson, E.C., Edwards, A.D., Rueckert, D., Sharp, D., Alexander, D., 2012. Hierarchy in anatomical brain networks derived from diffusion weighted images in 64 and 15 directions. Ann. BMVA 4, 1–21.

Deppe, M., Duning, T., Mohammadi, S., Schwindt, W., Kugel, H., Knecht, S., Ringelstein, E.B., 2007. Diffusion-tensor imaging at 3 T: detection of white matter alterations in neurological patients on the basis of normal values. Invest. Radiol. 42 (6), 338–345.

Drzezga, A., Becker, J.A., Van Dijk, K.R., Sreenivasan, A., Talukdar, T., Sullivan, C., Schultz, A.P., Sepulcre, J., Putcha, D., Greve, D., Johnson, K.A., Sperling, R.A., 2011. Neuronal dysfunction and disconnection of cortical hubs in non-demented subjects with elevated amyloid burden. Brain 134, 1635–1646.

Duning, T., Warnecke, T., Mohammadi, S., Lohmann, H., Schiffbauer, H., Kugel, H., Knecht, S., Ringelstein, E.B., Deppe, M., 2009. Pattern and progression of white-matter changes in a case of posterior cortical atrophy using diffusion tensor imaging. J. Neurol. Neurosurg. Psychiatry 80, 432–436.

Ewers, M., Sperling, R.A., Klunk, W.E., Weiner, M.W., Hampel, H., 2011. Neuroimaging markers for the prediction and early diagnosis of Alzheimer's disease dementia. Trends Neurosci. 34 (8), 430–442.

Fellgiebel, A., Müller, M.J., Wille, P., Dellani, P.R., Scheurich, A., Schmidt, L.G., et al., 2005. Color-coded diffusion-tensor-imaging of posterior cingulate fiber tracts in mild cognitive impairment. Neurobiol. Aging 26, 1193–1198.

Fouquet, M., Desgranges, B., Landeau, B., Duchesnay, E., Mézenge, F., de la Sayette, V., Viader, F., Baron, J.C., Eustache, F., Chételat, G., 2009. Longitudinal brain metabolic changes from amnestic mild cognitive impairment to Alzheimer's disease. Brain 132, 2058–2067.

Fox, M.D., Raichle, M.E., 2007. Spontaneous fluctuations in brain activity observed with functional magnetic resonance imaging. Nat. Rev. Neurosci. 8 (9), 700–711.

Gauthier, S., Reisberg, B., Zaudig, M., Petersen, R.C., Ritchie, K., Broich, K., Belleville, S., Brodaty, H., Bennett, D., Chertkow, H., Cummings, J.L., de Leon, M., Feldman, H., Ganguli, M., Hampel, H., Scheltens, P., Tierney, M.C., Whitehouse, P., Winblad, B., 2006. Mild cognitive impairment. Lancet 367, 1262–1270.

Good, P., 2004. Permutation, Parametric, and Bootstrap Tests of Hypotheses, 3rd ed. Springer, New York.

Greicius, M.D., Srivastava, G., Reiss, A.L., Menon, V., 2004. Default-mode network activity distinguishes Alzheimer's disease from healthy aging: evidence from functional MRI. Proc. Natl. Acad. Sci. U. S. A. 101, 4637–4642.

Greicius, M.D., Supekar, K., Menon, V., Dougherty, R.F., 2009. Resting-state functional connectivity reflects structural connectivity in the default mode network. Cereb. Cortex 19 (1), 72–78.

Hagmann, P., Cammoun, L., Gigandet, X., Meuli, R., Honey, C.J., Wedeen, V.J., Sporns, O., 2008. Mapping the structural core of human cerebral cortex. PLoS Biol. 6, e159.

Hahn, K., Prigarin, S., Rodenacker, K., Hasan, K., 2010. Denoising for diffusion tensor imaging with low signal to noise ratios: method and Monte Carlo validation. Int. J. Biomath. Biostat. 1 (1), 63–81.

Hahn, K., Prigarin, S., Hasan, K., 2013. Fitting of two-tensor models without ad hoc assumptions to detect crossing fibers using clinical DWI data. Magn. Reson. Imaging 31, 585–595. http://dx.doi.org/10.1016/j.mri.2012.10.013.

Hill, D.L.G., Batchelor, P., 2001. Registration methodology: concepts and algorithms. In: Hajnal, J.V., H. L. G., Hawkes, D.J. (Eds.), Medical Image Registration. CRC Press, pp. 40–70.

Huang, L., Wang, X., Baliki, M.N., Wang, L., Apkarian, A.V., Parrish, T.B., 2012. Reproducibility of structural, resting-state BOLD and DTI data between identical scanners. PLoS One 10 (7), e47684. http://dx.doi.org/10.1371/journal.pone.0047684.

Koay, C.G., Carew, J.D., Alexander, A.L., Basser, P.J., Meyerand, M.E., 2006. Investigation of anomalous estimates of tensor-derived quantities in diffusion tensor imaging. Magn. Reson. Med. 55, 930–936.

Lazar, M., Weinstein, D.M., Tsuruda, J.S., Hasan, K.M., Arfanakis, K., Meyerand, M.E., Badie, B., Rowley, H.A., Haughton, V., Field, A., Alexander, A.L., 2003. White matter tractography using diffusion tensor deflection. Hum. Brain Mapp. 18, 306–321.

Li, R., Wu, X., Fleisher, A.S., Reiman, E.M., Chen, K., 2013. Attention-related networks in Alzheimer's disease: a resting functional MRI study. Hum. Brain Mapp. (in press).

Lo, C.Y., Wang, P.N., Chou, K.H., Wang, J., He, Y., Lin, C.P., 2010. Diffusion tensor tractography reveals abnormal topological organization in structural cortical networks in Alzheimer's disease. J. Neurosci. 30, 16876–16885.

Mann, H.B., Whitney, D.R., 1947. On a test whether one of two random variables is stochastically larger than the other. Ann. Math. Stat. 18, 50–60.

McKhann, G., Drachman, D., Folstein, M., Katzman, R., Price, D., Stadlan, E.M., 1984. Clinical diagnosis of Alzheimer's disease: report of the NINCDS–ADRDA Work Group under the auspices of Department of Health and Human Services Task Force on Alzheimer's Disease. Neurology 34, 939–944.

Mormino, E.C., Smiljic, A., Hayenga, A.O., Onami, S.H., Greicius, M.D., Rabinovici, G.D., Janabi, M., Baker, S.L., Yen, I.V., Madison, C.M., Miller, B.L., Jagust, W.J., 2011. Relationships between beta-amyloid and functional connectivity in different components of the default mode network in aging. Cereb. Cortex 21, 2399–2407.

Morris, J.C., 1993. The Clinical Dementia Rating (CDR): current version and scoring rules. Neurology 43, 2412–2414.

Morris, J.C., Heyman, A., Mohs, R.C., Hughes, J.P., van Belle, G., Fillenbaum, G., Mellits, E.D., Clark, C., 1989. The Consortium to Establish a Registry for Alzheimer's Disease (CERAD). Part I. Clinical and neuropsychological assessment of Alzheimer's disease. Neurology 39, 1159–1165.

Neubert, K., Brunner, E., 2006. A studentized permutation test for the nonparametric Behrens–Fisher problem. Comput. Stat. Data Anal. 51, 5192–5204.

Neufang, S., Akhrif, A., Riedl, V., Forstl, H., Kurz, A., Zimmer, C., Sorg, C., Wohlschlager, A.M., 2011. Disconnection of frontal and parietal areas contributes to impaired attention in very early Alzheimer's disease. J. Alzheimers Dis. 25, 309–321.

Neuhäuser, M., Ruxton, G.D., 2009. Distribution-free two-sample comparisons in the case of heterogeneous variances. Behav. Ecol. Sociobiol. 63, 617–623.

Pievani, M., de Haan, W., Wu, T., Seeley, W.W., Frisoni, G.B., 2011. Functional network disruption in the degenerative dementias. Lancet Neurol. 10, 829–843.

Press, W., Teukolsky, S.A., Vetterling, W.T., Flannery, B.P., Press, W., Teukolsky, S.A., Vetterling, W.T., Flannery, B.P., 1992. Numerical Recipes, second ed. Cambridge University Press.

Rorden, C., Bonilha, L., Nichols, T.E., 2007. Rank-order versus mean based statistics for neuroimaging. NeuroImage 35, 1531–1537.

Sexton, C.E., Kalu, U.G., Filippini, N., Mackay CE Ebmeier, K.P., 2011. A meta-analysis of diffusion tensor imaging in mild cognitive impairment and Alzheimer's disease. Neurobiol. Aging 32 (2322.e5-2322.18).

Shao, J.M.N., Yang, Q., Feng, J., Plant, C., Böhm, C., Förstl, H., Kurz, A., Zimmer, C., Meng, C., Riedl, V., Wohlschläger, A.M., Sorg, C., 2012. Prediction of Alzheimer's disease using individual structural connectivity networks. Neurobiol. Aging 33 (2), 2756–2765.

Sheline, Y.I., Raichle, M.E., 2013. Resting State Functional Connectivity in Preclinical Alzheimer's Disease. Biol. Psychiatry. http://dx.doi.org/10.1016/j.biopsych.2012.11.028 (in press).

Smith, S.M., Fox, P.T., Miller, K.L., Glahn, D.C., Fox, P.M., Mackay, C.E., Filippini, N., Watkins, K.E., Toro, R., Laird, A.R., Beckmann, C.F., 2009. Correspondence of the brain's functional architecture during activation and rest. Proc. Natl. Acad. Sci. U. S. A. 106, 13040–13045.

Soldner, J., Meindl, T., Koch, W., Bokde, A.L.W., Reiser, M.F., Möller, H.J., Bürger, K., Hampel, H., Teipel, S.J., 2012. Structural and functional neuronal connectivity in Alzheimer's disease. A combined DTI and fMRI study. Nervenarzt 83, 878–887.

Sorg, C., Riedl, V., Muhlau, M., Calhoun, V.D., Eichele, T., Laer, L., Drzezga, A., Forstl, H., Kurz, A., Zimmer, C., Wohlschlager, A.M., 2007. Selective changes of resting-state networks in individuals at risk for Alzheimer's disease. Proc. Natl. Acad. Sci. U. S. A. 104, 18760–18765.

Sorg, C., Riedl, V., Perneczky, R., Kurz, A., Wohlschlager, A.M., 2009. Impact of Alzheimer's disease on the functional connectivity of spontaneous brain activity. Curr. Alzheimer Res. 6, 541–553.

Sorg, C., Manoliu, A., Neufang, S., Myers, N., Peters, H., Schwerthöffer, D., Scherr, M., Mühlau, M., Zimmer, C., Drzezga, A., Förstl, H., Bäuml, J., Eichele, T., Wohlschläger, A.M., Riedl, V., 2013. Increased intrinsic brain activity in the striatum reflects symptom dimensions in schizophrenia. Schizophr. Bull. 39 (2), 387–395.

Sperling, R.A., Laviolette, P.S., O'Keefe, K., O'Brien, J., Rentz, D.M., Pihlajamaki, M., Marshall, G., Hyman, B.T., Selkoe, D.J., Hedden, T., Buckner, R.L., Becker, J.A., Johnson, K.A., 2009. Amyloid deposition is associated with impaired default network function in older persons without dementia. Neuron 63, 178–188.

Stahl, R., Dietrich, O., Teipel, S.J., Hampel, H., Reiser, M.F., Schoenberg, S.O., 2007. White matter damage in Alzheimer disease and mild cognitive impairment: assessment with diffusion-tensor MR imaging and parallel imaging techniques. Radiology 243, 483–492.

Stam, C.J., Reijneveld, J.C., 2007. Graph theoretical analysis of complex networks in the brain. Nonlin Biomed Phys 1–19. http://dx.doi.org/10.1186/1753-4631-1-3.

van den Heuvel, M.P., Mandl, R.C., Kahn, R.S., Hulshoff Pol, H.E., 2009. Functionally linked resting-state networks reflect the underlying structural connectivity architecture of the human brain. Hum. Brain Mapp. 30, 3127–3141.

Wee, C.Y., Yap, P.-T., Zhang, D., Denny, K., Browndyke, J.N., Potter, G.G., Welsh-Bohmer, K.A., Wang, L., Shen, D., 2012. Identification of MCI individuals using structural and functional connectivity networks. NeuroImage 59, 2045–2056.

Westfall, P.H., Troendle, J.F., 2008. Multiple testing with minimal assumptions. Biom. J. 50, 745–755.

Westfall, P., Young, S.S., 1993. Resampling Based Multiple Testing. John Wiley & Sons, New York.

Zhou, Y., Dougherty, J.H.J., Hubner, K.F., Bai, B., Cannon, R.L., Hutson, R.K., 2008. Abnormal connectivity in the posterior cingulate and hippocampus in early Alzheimer's disease and mild cognitive impairment. Alzheimers Dement. 4, 265–270.